Metals & corrosion

Irradiation damage and swelling of carbon-doped Fe$_{38}$Mn$_{40}$Ni$_{11}$Al$_4$Cr$_7$ high-entropy alloys under heavy ion irradiation at elevated temperature

Shangkun Shen[1,3], Feida Chen[1,3,*], Xiaobin Tang[1,2,*], Guojia Ge[1], Jing Gao[1], and Zhangjie Sun[1]

[1] Department of Nuclear Science and Technology, Nanjing University of Aeronautics and Astronautics, Nanjing 211106, China
[2] Key Laboratory of Nuclear Technology Application and Radiation Protection in Astronautics (Nanjing University of Aeronautics and Astronautics), Ministry of Industry and Information Technology, Nanjing 211106, China
[3] Jiangsu Engineering Laboratory of Nuclear Energy Equipment Materials, Nanjing 211106, China
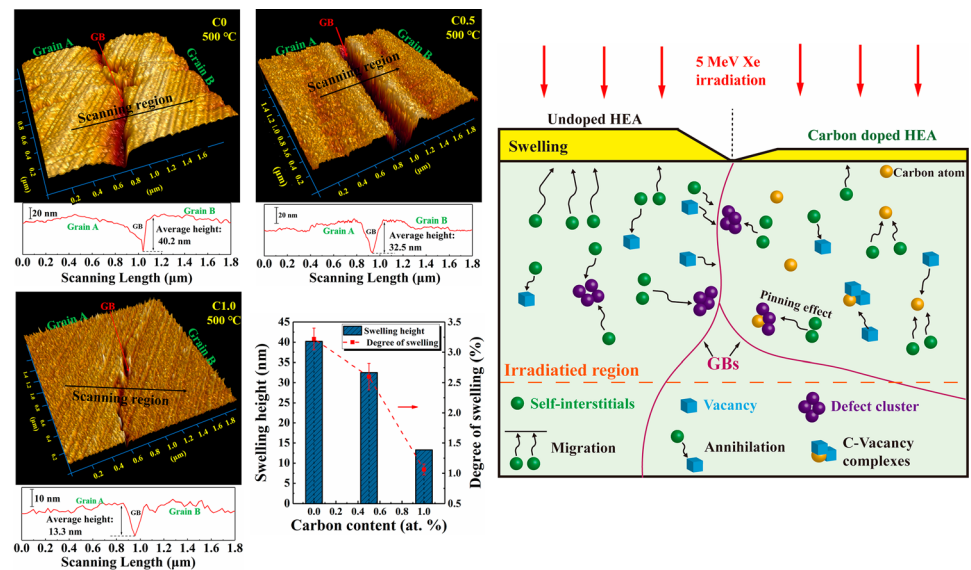
ABSTRACT

Interstitial strengthening is one of the main approaches to improving the mechanical properties of high-entropy alloys (HEAs), but its effects on the irradiation resistance of HEAs need further study. Here, we investigated the irradiation-induced defects and swelling of Fe$_{38}$Mn$_{40}$Ni$_{11}$Al$_4$Cr$_7$ HEAs with different carbon contents under 5 MeV Xe^{23+} irradiation at 300 °C and 500 °C. Results show that the irradiation-induced swelling was significantly suppressed as the carbon content increased. Under the observation of TEM, the size of irradiation-induced dislocation loops also decreases with increasing carbon content. By comparing the effects of carbon content at different temperatures on the evolution of defects, the pinning effect of interstitial carbon on irradiation-induced defects of HEAs was proposed and analyzed. Carbon atoms, which are stabilized in the octahedron clearance of HEAs with FCC structure, not only promote the recombination of point defects by enhancing the sluggish diffusion effect of HEAs, but also pin the common 1/3 <111> faulted loops caused by irradiation. This pinning effect is the main mechanism of interstitial carbon for improving the irradiation resistance of HEAs below 300 °C. In summary, this study provides an essential experimental basis for the irradiation effects of carbon-doped HEAs and strives to reveal the effect of interstitial carbon on irradiation-induced defects at different temperatures.

GRAPHICAL ABSTRACT

Introduction

Structural materials for nuclear reactor applications are exposed to prolonged irradiation at elevated temperatures, which could cause the swelling [1, 2], hardening [1, 3], and irradiation assisted stress corrosion cracking [4] of materials, thereby endangering the safe and long-term operation of nuclear reactors. According to previous research, high-entropy alloys (HEAs) are considered one of the candidate structural materials for next-generation nuclear reactors due to their superior mechanical properties [5, 6] and good irradiation resistance [7, 8] compared with those of conventional metal materials. The current research on the irradiation resistance of HEAs mainly focuses on the effects of irradiation temperature and dose [9, 10], alloying elements [11, 12], and so on; however, studies about the effects of interstitials on the irradiation resistance of HEAs are very limited.

Recently, carbon-doped HEAs have attracted widespread attention for various applications due to the combination of their excellent mechanical properties and chemical stability at normal and elevated temperatures [13–15]. In addition, Lu et al. [16] recently reported that the interstitial carbon atoms in

FeMnNiCoCr HEA enhance the recombination of point defects and inhibit the accumulation of vacancies under proton irradiation, which were observed using positron annihilation spectroscopy. Similarly, in our previous experiment [17], we found that carbon-doped HEAs exhibit improved irradiation resistance in comparison with undoped HEAs, especially inhibiting the growth of irradiation defects and irradiation hardening under heavy ion irradiation at room temperature. The specific data are shown in Figs. S3 and S4 in *Supplementary material*.

To further evaluate the feasibility of using carbon-doped HEAs as structural materials in nuclear applications, their irradiation effects at elevated temperature, such as irradiation-induced swelling, segregation, and hardening, need to be studied. Based on previous reports, it is demonstrated that the unique chemical disorder and lattice distortion of HEAs reduce the mobility of interstitial atoms [18] that increase the defect formation barrier and promote the annihilation of irradiation-induced defects. Furthermore, as a widely used approach to strengthening alloys, minor interstitial carbon addition could increase the chemical disorder and lattice distortion, which may further enhance the inherent sluggish diffusion effect of HEAs and improve their

irradiation resistance. Moreover, interstitial carbon atoms in NiFe-based alloy have been proved to interact with irradiation-induced vacancies and form C-vacancy complexes [19], which could increase the barrier of vacancy migration and suppress the growth of irradiation-induced voids [20, 21]. In addition, we believe that pinning is the main effect of interstitial carbon on large-sized irradiation defects, such as dislocation loops and net dislocation. This work seeks to confirm this view by changing the irradiation temperature.

In our present work, the evolution of irradiation-induced defects and swelling in FeMnNiAlCr HEAs with and without carbon doping irradiated at elevated temperatures is characterized by using transmission electron microscopy (TEM) and atomic force microscopy (AFM). As for choosing $Fe_{38}Mn_{40}Ni_{11}Al_4Cr_7$ as the HEA matrix, there are two main reasons: on the one hand, the carbon-doped HEAs are expected to be used as structural material in nuclear system; thus, the superiority of their mechanical properties is a more significant concern in engineering field. Based on the reports of Wang et al. [22, 23], the carbon-doped $Fe_{40.4}Ni_{11.3}Mn_{34.8}Al_{7.5}Cr_6$ HEAs have excellent mechanical properties that may be able to meet the requirements of structural materials. On the other hand, Co and Ni elements are unfavorable for nuclear applications due to their high neutron activation. Therefore, we chose the HEAs without Co element and a small amount of Ni element, which are similar to the HEAs with excellent mechanical properties in Wang's work. In addition, the effects of the varying carbon contents in HEAs on defects evolution at different irradiation temperatures are investigated.

Methods

Three types of $Fe_{38}Mn_{40}Ni_{11}Al_4Cr_7$ HEAs with 0 at.%, 0.5 at.%, and 1.0 at.% carbon doping contents were used in the present study. The ingots were prepared by the vacuum levitation melting process and then re-melted at least three times to ensure homogeneity before drop cast into a copper mold. Subsequently, all the ingots were processed into 1 cm × 1 cm × 0.1 cm sheets by wire electrical discharge machining. The specific chemical compositions of the alloys are found in Tab. S1 in *Supplementary material*. In the following, **C0**, **C0.5**, and

C1.0 represent the samples with 0 at.%, 0.5 at.%, and 1.0 at.% carbon doping contents, respectively. The alloys were irradiated with 5 MeV Xe^{23+} ion beam to fluences of 1.4×10^{15} cm^{-2} at 300 °C and 500 °C on the 320-kV platform at the Institute of Modern Physics, Chinese Academy of Sciences (CAS). The corresponding irradiation-induced damage profile and the Xe concentration were calculated using SRIM-2013 at the Quick Kinchin-Pease mode. Given the negligible effect of trace carbon on the calculation results of SRIM, only the result of C0.5 is shown in Fig. 1d. During irradiation, the particle flux was set to $\sim 1.38 \times 10^{11}$ ions/cm^2 s (3.75×10^{-4} dpa/s). The irradiation temperatures are approximately equal to $0.25T_m$ and $0.40T_m$ for all the alloys (T_m is the melting point of the material). To ensure the same irradiation conditions, the three samples were pieced together in the middle of the irradiation target with the ion beam at spot size of 1.8×1.8 cm^2. The heating rate of the sample target was controlled to 1 °C per 5 s with vacuum in the target chamber maintained at approximately 10^{-6} Pa.

Cross-sectional TEM foils were prepared through the focused ion beam (FIB) lift-out technique on a FEI Helios workstation at Shanghai Institute of Optics and Fine Mechanics, CAS. During the FIB process, 30 and 5 keV Ga ions were used to thin the foils and remove the amorphous layer caused by the FIB. In the final milling, 2-keV Ga ions were used to reduce the effect of FIB damage on the TEM foils. TEM (FEI Talos F200X of Suzhou Institute of Nano-Tech and Nano-Bionics, CAS) with a two-beam diffracting condition in the bright field (BF) was adopted to characterize the microstructures of the irradiation-induced defects in irradiated samples. Considering that the dislocation loops in f.c.c alloys caused by irradiation are mainly faulted loops with **b** = 1/3 <111> and perfect loops with **b** = 1/2 <110>, the diffraction vector **g** = 200 is not extinct with the above dislocation loops, so the both types of dislocation loops can be observed in the field view of TEM. The size and density of the dislocation loops were estimated in the Nano-measurement software, and the data for each sample were taken from at least 10 TEM images to prevent accidents. In addition, AFM (Bruker Dimension Icon) was adopted to measure the step height of grain boundaries (GBs) in irradiation regions. Among them, the average step heights of GBs were measured from at least 10 different positions of the irradiated region for each
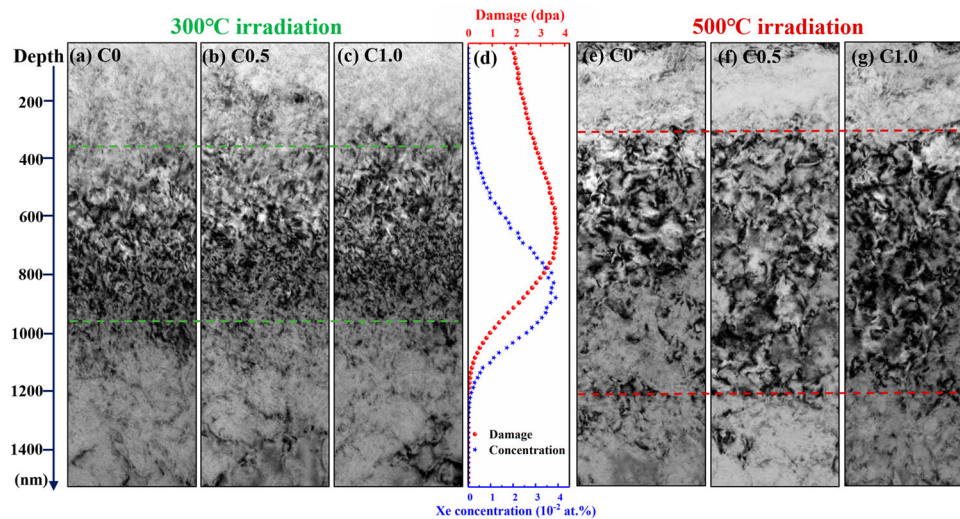
Figure 1 Cross-sectional BF TEM images of the C0, C0.5, and C1.0 samples irradiated with 5 MeV Xe^{23+} to a fluence of 1.4×10^{15} cm^{-2} at 300 °C and 500 °C. **a**–**c** are the case of 300 °C irradiation condition. **e**–**g** are the case of 500 °C irradiation condition. **d** is the calculation result of SRIM for the C0.5 sample corresponding to the above irradiation condition. The defect distributions of the samples are consistent with the SRIM calculation result.

sample to avoid accidents. The changes in height at different measurement positions are presented as standard deviations.

Results and discussion

Irradiation-induced defects

Figure 1a–c, e–g shows the cross-sectional BF TEM images of the irradiation-induced damage bands in the C0, C0.5, and C1.0 samples irradiated at 300 °C and 500 °C, respectively. In the case of irradiation at 300 °C, the damage bands of the samples were mainly concentrated in the depth region of approximately 400–1000 nm, while under the 500 °C irradiation condition, the irradiation-induced defects were scattered in a deeper region than the case of 300 °C irradiation, approximately 400–1200 nm. As shown in Fig. 1d, the defect distributions in both cases are within the theoretical damage depth range calculated by SRIM. However, the distribution of defects expanded as the temperature of irradiation increased, which may be attributed to the increased mobility of defects with increasing temperature. Clearly, whether the samples were irradiated at 300 °C or 500 °C, typical dislocation loops, such as 1/3 <111> faulted loops, are the main visible defects, while no void was observed in our work. Previous reports [24, 25] indicate that in conventional metal materials,

vacancies can gather to form clusters or voids when the irradiation temperature T = 0.23–0.35 T_m (T_m is the melting point of the material) and continue to grow until saturation when T > 0.35 T_m. In our work, 300 °C and 500 °C, respectively, correspond to approximately 0.25 T_m and 0.4 T_m, but no voids were observed. This may be attributed to the unique lattice distortion and sluggish diffusion effect of HEAs [26], which further hinder the migration of vacancies, thereby suppressing the formation and growth of voids at elevated temperatures. Furthermore, irradiation-induced dislocation loops tend to accumulate and grow into large-sized defects. The comparison of the defect distribution of the samples with different carbon contents at the same irradiation condition indicates that the damage bands of the samples were consistent in the case of 300 °C irradiation, but when the temperature increased to 500 °C, the C0.5 and C1.0 samples exhibited more dispersed defect distributions than that of C0 sample. This phenomenon suggests that interstitial carbon atoms may inhibit the accumulation of irradiation-induced defects, resulting in the dispersed defects of carbon-doped samples, and the effect of interstitial carbon on distribution of defects was more significant at higher temperature in our work. To reveal the specific effects of interstitial carbon on irradiation-induced defects, we investigated the microstructure and evolution of defects in
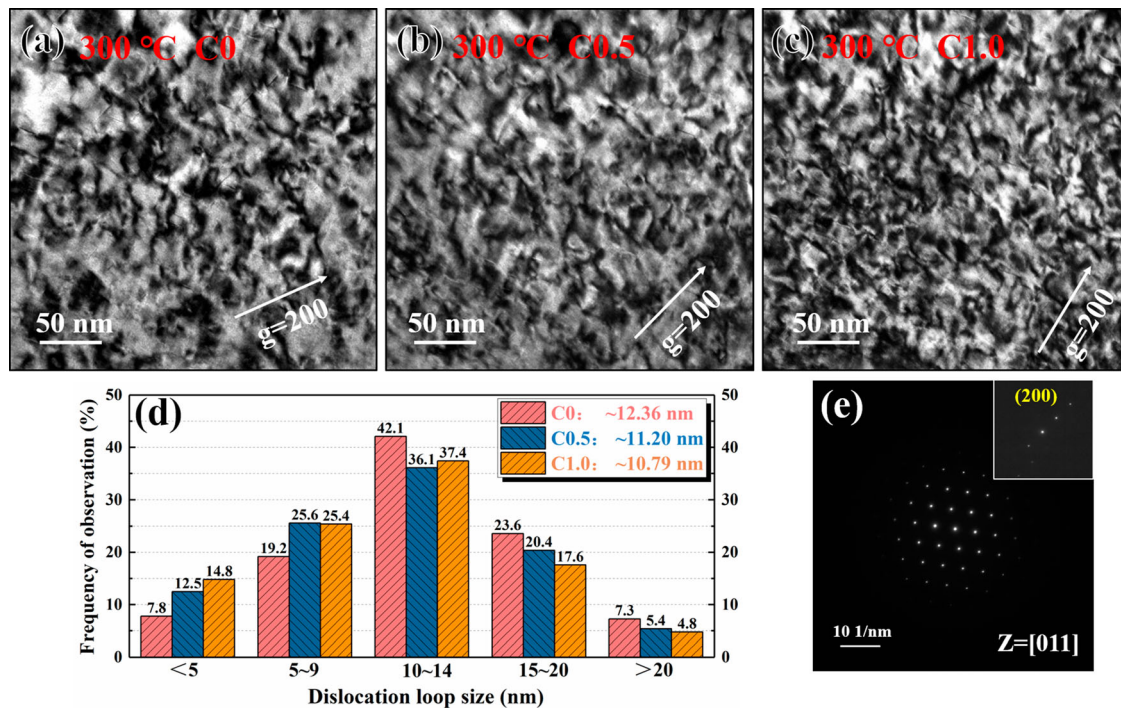
Figure 2 Enlarged BF TEM images for the damage peak regions of **a** C0, **b** C0.5, and **c** C1.0 samples irradiated with 5 MeV Xe^{23+} to a fluence of 1.4×10^{15} cm^{-2} at 300 °C. **d** is statistical result for the size distribution of dislocation loops in C0, C0.5, and C1.0 samples based on at least 10 TEM images. **e** are SAED patterns, showing the two-beam diffracting condition of TEM images: all the images were taken near the [011] zone axis with g = 200.

the samples with different carbon contents at 300 °C and 500 °C irradiation conditions.

Figure 2a–c shows the enlarged TEM images of the irradiation-induced damage bands of the C0, C0.5, and C1.0 samples irradiated at 300 °C. All these TEM images were taken near the [011] zone axis with **g** = 200 (as shown in Fig. 2e). In this case, the damage bands were mainly composed of high-density dislocation loops, and the number density of the dislocation loops increased visually with the carbon content. According to a previous report [27], these loops are considered to be interstitial-type dislocation loops, which are formed by the accumulation of interstitial atoms. We counted the dislocation loops in the damage bands of the C0, C0.5, and C1.0 samples and measured their size, as shown in Fig. 2d. The average sizes of dislocation loops in the three samples were estimated to be 12.06, 11.20, and 10.79 nm, respectively. Notably, the distributions of the dislocation loop sizes of C0, C0.5, and C1.0 samples were all mainly concentrated in the 10–14 nm interval, accounting for 42.1%, 36.1%, and 37.4%, respectively. However, Compared with C0 sample, the proportions of small-sized (< 10 nm) dislocation loops in the

C0.5 and C1.0 samples were higher. The proportions of the large-sized (> 14 nm) dislocation loops in the C0, C0.5, and C1.0 samples were estimated as 30.9%, 25.8%, and 22.4%, respectively. These results indicate that the carbon-doped HEAs exhibited smaller defect sizes under irradiation at 300 °C than the undoped sample. Since the effect of trace carbon addition on the formation of irradiation-induced point defects is negligible, we assumed that the number of initial point defects (self-interstitials and vacancies) in C0, C0.5, and C1.0 samples is the same under the same irradiation condition. In this case, interstitial carbon atoms provided nucleation sites for the dislocation loops and inhibited their movement, resulting in higher number densities and smaller sizes of dislocation loops in the doped samples than those in the undoped sample. In addition, the mobility of large-sized dislocation loops is originally weaker than that of small-sized ones, and a large-sized dislocation loop may be pinned by multiple interstitial carbons. However, the small-sized dislocation loops are highly mobile at elevated temperatures. Considering the evolution of dislocation loops, the movement and aggregation of small-sized dislocation loops are the

main reason for the growth of dislocation loops with large sizes. Comparing the sizes of dislocation loops in C0.5 and C1.0 samples, we found that as the carbon content increased, the proportion of large-sized dislocation loops decreased. This phenomenon suggested that as the carbon content increases, the pinning strength of interstitial carbons on small-sized dislocation loops was enhanced, which hindered the movement and aggregation of these dislocation loops.

As shown in Fig. 3a–c, in the case of 300 °C irradiation, in addition to the identifiable dislocation loops in the damage bands, a bulk of black dots accompanied with some dislocation lines were found in the region depth of 1100–1400 nm, which is beyond the damage region calculated by SRIM. This may be due to the fact that small-sized defect clusters are more mobile than large-sized defects; therefore, small-sized defects tend to migrate to deeper locations, even beyond the irradiation layer [18]. As shown in Fig. 3d, the SAED pattern shows a single-phase FCC structure, thus indicating the black dots were not nano-precipitates. Notably, under the same diffraction vector, the influence of different zone axes

on TEM images is negligible in our work. These black dots are considered as clusters or small-sized dislocation loops composed of migrating interstitial atoms, and the morphology of these irradiation-induced black dots is consistent with previous studies on austenitic stainless steels irradiated with neutrons and heavy ions at low temperatures (below 350 °C) [2, 28]. We made statistics and comparisons of the black dots for the samples with different carbon contents, as shown in Fig. 3e. Considering that some black dots with sizes of less than 3 nm cannot be observed or accurately identified in the TEM images, the average size of the black dots calculated by TEM images may be larger than the actual situation. The average sizes of black dots in the irradiated C0, C0.5, and C1.0 samples were estimated to be 8.56, 5.89, and 5.04 nm, respectively, which are consistent with the trend of the size difference of dislocation loops in the damage bands. Specifically, as the carbon content of the samples increased, the average size of black dots decreased and the number density increased. This phenomenon is attributed to the reason that the interstitial carbon atoms weakened the mobility of self-interstitial atoms and promoted their
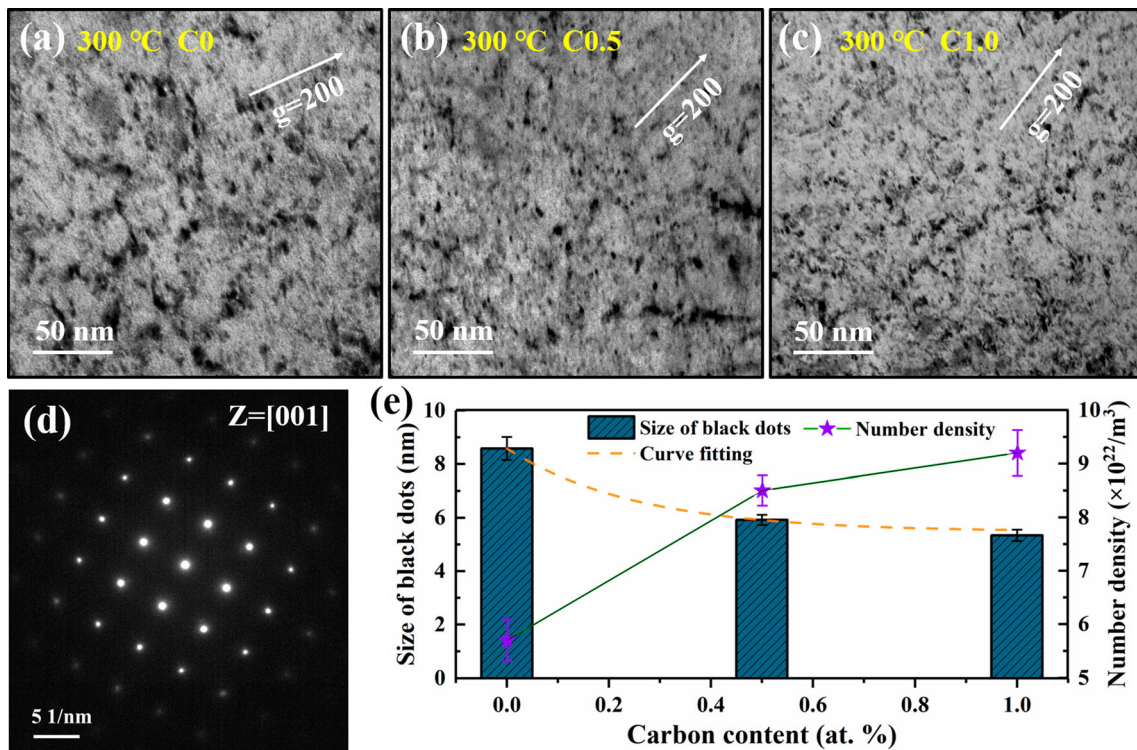

Figure 3 BF TEM images of the black dots in **a** C0, **b** C0.5, and **c** C1.0 samples irradiated with 5 MeV Xe^{23+} to a fluence of 1.4×10^{15} cm^{-2} at 300 °C. **d** is SAED pattern shows [001] zone axis with no detectable precipitation. **e** is the mean size and number density of the black dots in the irradiated samples with different carbon contents.

annihilation during the 3D migration path, reducing the number of migratable defects. However, specific numerical values of the migration energy of self-interstitial atoms in the samples with different carbon contents are difficult to provide, thus requiring further verification by simulation methods.

As shown in Fig. 4a–c, typical large-sized 1/3 <111> faulted loops are distributed in the damage bands of the samples irradiated at 500 °C. The average sizes of the dislocation loops in C0, C0.5, and C1.0 samples were estimated to be 17.5, 15.8, and 15.2 nm, respectively, and the trend of this result is similar to that in the case of 300 °C irradiation. However, in the case of 500 °C irradiation, the difference in average defect sizes of the C0.5 and C1.0 samples was very small because the pinning effects of interstitial carbon on irradiation-induced dislocation loops were affected by temperature. Specifically, when the irradiation temperature is high enough, interstitial carbon atoms begin to migrate [29], causing the invalidation of the pinning effect of interstitial carbon on dislocation loops. Moreover, the elevated temperature intensified

the thermal motion of molecules and reduced the migration energy of irradiation defects, which may result in the unpinning of many dislocation loops. In this case, the content of interstitial carbon would no longer influence the pinning strength of the dislocation loops, greatly weakening the response of the dislocation loop size to the carbon content.

Stacking fault tetrahedron (SFT) is a kind of vacancy-type and stable defect in FCC crystal, which is formed by the migration of vacancy clusters or the evolution of Frank loops. As shown in Figs. 5a, b, SFTs were observed in the C0 samples irradiated at 300 °C and 500 °C, while no SFT was observed in the C0.5 and C1.0 samples at both 300 °C and 500 °C irradiation temperatures. This may be attributed to the reason that interstitial carbon atoms had inhibitory effects on the above two formation mechanisms of SFTs. Firstly, interstitial carbon atoms could combine with the vacancies to form C-vacancy complexes, thereby inhibiting the accumulation and movement of vacancies. Reportedly, the vacancies in the austenitic steel can stably bind two carbon atoms
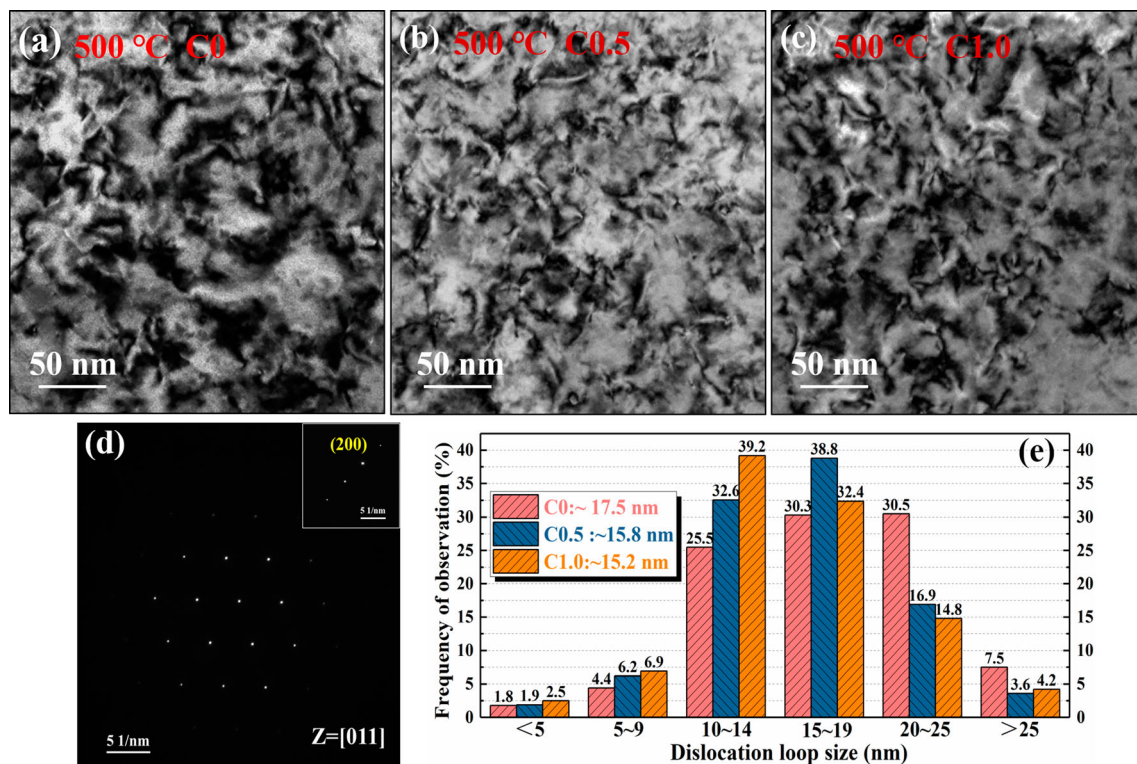

Figure 4 Enlarged BF TEM images for the damage peak regions of **a** C0, **b** C0.5, and **c** C1.0 samples irradiated with 5 MeV Xe^{23+} to a fluence of 1.4×10^{15} cm^{-2} at 500 °C. **d** is SAED patterns, showing the two-beam diffracting condition of TEM images: all the images were taken near the [011] zone axis with g = 200. **e** is statistical result for the size distribution of dislocation loops in C0, C0.5, and C1.0 samples based on at least 10 TEM images.
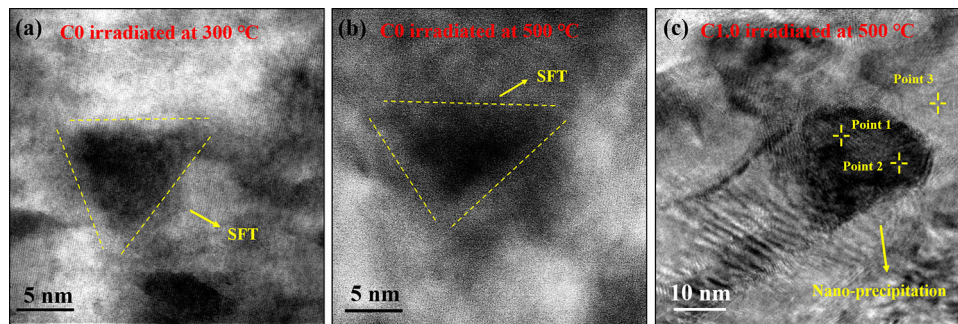
Figure 5 Stacking fault tetrahedrons (SFTs) of the C0 sample irradiated with 5 MeV Xe^{23+} to a fluence of 1.4×10^{15} cm^{-2} at **a** 300 °C and **b** 500 °C. **c** is a nano-precipitation of C1.0 sample irradiated with 5 MeV Xe^{23+} to a fluence of 1.4×10^{15} cm^{-2} at 500 °C.

with a binding energy of up to 0.4 eV [30]. In addition, the carbon atoms located in the octahedral interstitial position have a significant pinning effect on the 1/3 <111> faulted loops, hindering their evolution to SFTs. The average sizes of SFTs in C0 irradiated at 300 °C and 500 °C were estimated as 7.23 and 8.84 nm, respectively. This is due to the enhanced mobility of vacancies and dislocation loops at 500 °C compared with those at the 300 °C condition. However, the number densities of the SFTs in the C0 samples were very low, only approximately 2.7×10^{8} m^{-3} and 6.3×10^{7} m^{-3}, and their interaction with irradiation-induced dislocation loops was ignored in our work. In addition, as shown in Fig. 5c, we found some nano-precipitation with an average size of approximately 10 nm in the C1.0 sample irradiated at 500 °C. Table 1 shows the EDS results for the nano-precipitates and matrix in the C1.0 sample. It can be confirmed that the precipitates are carbides rich in Mn and Cr elements, and the content of each element in the matrix was basically consistent with expectations. According to a previous study [29], C-vacancy complexes may dissociate at elevated temperature. In this case, carbon atoms may undergo long-range migration [31] due to the increased thermal activation caused by thermal spike of irradiation and combine with Mn and Cr atoms to form nano-sized carbides. Similar to the SFTs in the C0 sample, the nano-precipitates in the C1.0 sample existed in small amounts near the surface. Thus, we ignored
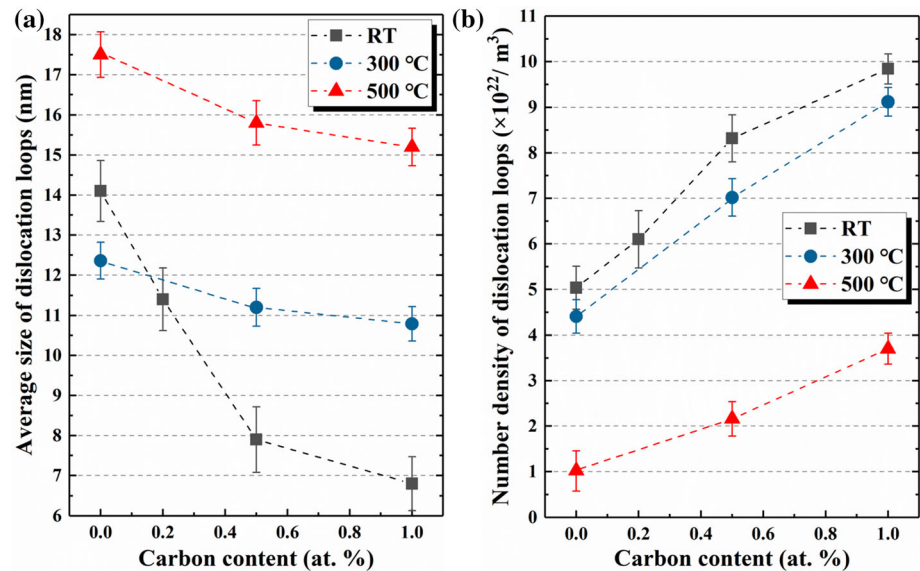
their effect on the evolution of irradiation-induced defects in our work.

In Fig. 6, we provide the average sizes and densities of the dislocation loops in the samples irradiated at room temperature (RT) [17], 300 °C and 500 °C to systematically investigate the influence of carbon content and irradiation temperature on the irradiation-induced dislocation loops and reveal the effect of interstitial carbon at different irradiation temperatures. It can be found that as the irradiation temperature increases, the size of the dislocation loops increases and the number density decreases. However, the average dislocation loop size of the C0 sample irradiated at 300 °C was smaller than that of the C0 irradiated at room temperature. This phenomenon may be because the mobility of self-interstitial atoms and vacancies at 300 °C is enhanced compared to RT, which promotes the recombination of defect pairs, thereby reducing the defect size of the C0 sample irradiated at 300 °C. However, in the case of carbon-doped samples, the pinning and inhibition effect of interstitial carbon on defect migration would compete with the defect evolution dominated by temperature. This competition weakens the effect of irradiation temperature on the recombination of point defects, resulting in a positive correlation between the defect size and the irradiation temperature. In addition, under the same irradiation conditions including the cases of RT, 300 °C and 500 °C irradiation, as the carbon content increased, the size

Table 1 EDS point scan result of C1.0 sample irradiated at 500 °C: Point 1 and point 2 are precipitated particles; point 3 is the matrix (points 1–3 are identified from Fig. 5c)

	Fe (at.%)	Mn (at.%)	Ni (at.%)	Al (at.%)	Cr (at.%)	C (at.%)
Point 1	8.56	56.11	1.43	1.27	10.33	21.30
Point 2	10.76	52.61	3.77	2.21	10.79	18.86
Point 3	35.85	39.88	10.54	4.47	5.98	3.28

Figure 6 a Mean size and **b** number density of irradiation-induced dislocation loops of the samples with different carbon contents under room temperature (RT) [17], 300 °C and 500 °C irradiation conditions. The irradiation fluence of all the above samples is 1.4×10^{15} cm^{-2}, which corresponds to the peak damage dose of 3.8 dpa. The images and data of the irradiated samples at RT are found in *Supplementary material*.

of the dislocation loops decreased and the number density increased, proving that interstitial carbon atoms inhibit the growth of irradiation-induced defects and improve the irradiation resistance of carbon-doped HEAs.

Irradiation-induced swelling

Irradiation-induced swelling of material is remarkable at elevated temperature (0.3–0.6 T_m, where T_m is the melting point of the material), negatively affecting the performance of structural materials in nuclear applications. According to previous reports [32, 33], there are two causes of irradiation swelling: void-induced swelling and bubble-induced swelling. The degree of swelling strongly depends on the density and size of the voids or bubbles. Considering that the Xe irradiation fluence of all the samples is 1.4×10^{15} cm^{-2} and no Xe bubbles were observed in the TEM images, the swelling of the irradiated samples in our work is considered to be caused by the voids and the migration of interstitial atoms. In addition, Terasawa et al. [32] reported that GBs exhibit a different step structure from matrix under N$^+$ irradiation at 773 K, which could reflect the irradiation swelling of the sample. This is because the GBs absorb a large number of interstitials and vacancies and prompt them to annihilate there, resulting in no evolution of irradiation-induced defects at GBs [34]. On the basis of the above research results, we explored the swelling at the GBs of the samples with different carbon contents after Xe^{23+}

irradiation at elevated temperature, so as to explain the effect of carbon doping on irradiation-induced swelling. However, we did not find any detectable swelling of the samples irradiated at 300 °C ($\sim 0.25\ T_m$). Thus, we only provide the swelling of the samples irradiated at 500 °C.

Figure 7a–c shows 3D AFM images for the GBs of the C0, C0.5, and C1.0 samples irradiated at 500 °C. Among them, the illustrations are corresponding cross-sectional data of the scanning line in the AFM images. Clearly, the characteristic grooves at the GBs were observed in all the samples, while different volume swelling appeared on both sides of the GBs in each sample. For ease of expression, we defined the average height above the both sides of grooves as the GBs' step height (H$_{GBs}$), as shown in Fig. 7d. To avoid accidental experimental data, we used the above method to test 10 different GBs of each sample and calculated the average swelling height. The average swelling heights of the C0, C0.5, and C1.0 sample were estimated to be 40.2 nm, 32.5 nm, and 13.3 nm, respectively. Furthermore, on the basis of the calculation result of SRIM and TEM observation, the depth of irradiated region (h_{irr}) was determined to be approximately 1250 nm. Thus, the degrees of swelling at GBs ($\Delta h = H_{GBs}/h_{irr} \times 100\%$) were calculated to be 3.22%, 2.60%, and 1.06% for the C0, C0.5, and C1.0 samples, respectively. Notably, the swelling degree of C1.0 sample dropped to 33% of the C0 sample, suggesting that the volume swelling of the sample was suppressed under Xe^{23+} irradiation at 500 °C with increasing the carbon concentration. We
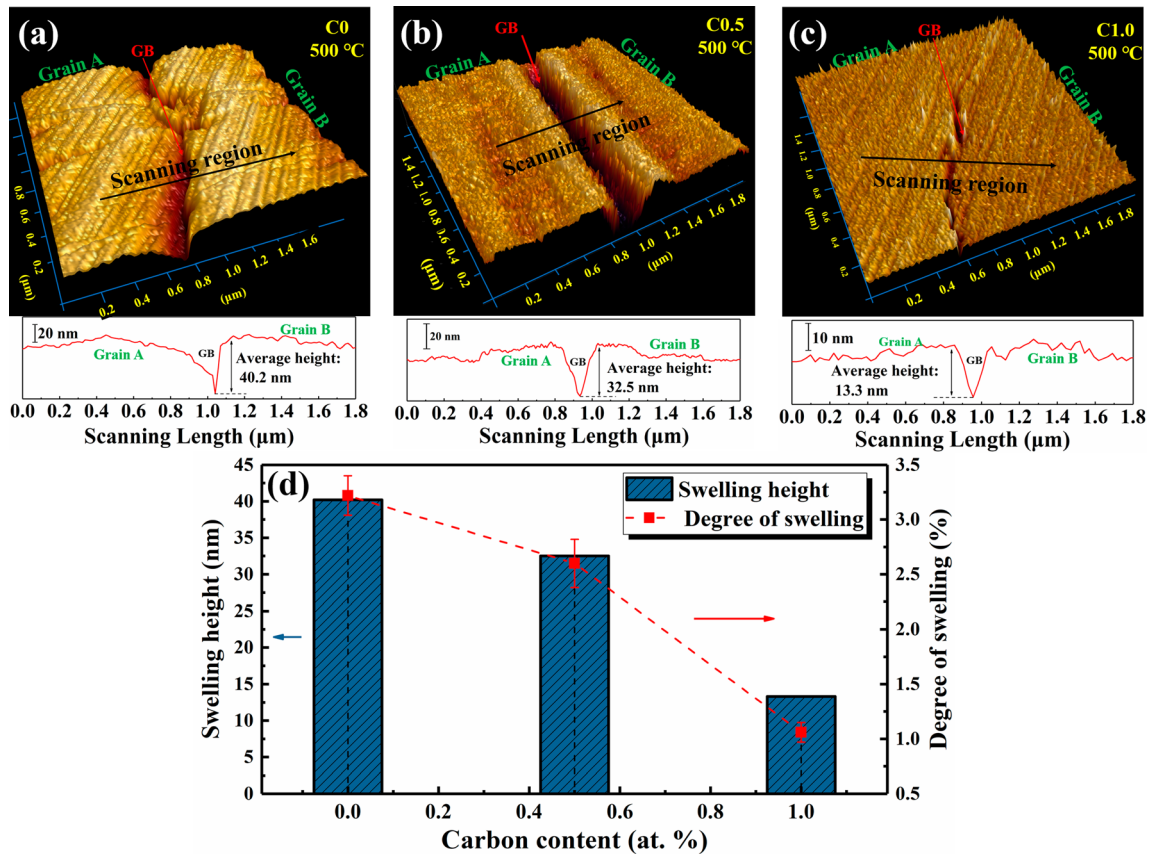
Figure 7 3D AFM images for the GBs of the **a** C0, **b** C0.5, and **c** C1.0 samples irradiated at 500 °C. The insets in **a**–**c** are the data result corresponding to the scanning line. **d** shows the swelling height and degree of swelling of the samples with different carbon contents irradiated at 500 °C.

estimated the Δh/dpa (%/dpa) values of the irradiated C0, C0.5, and C1.0 samples as 0.85, 0.68, and 0.28, respectively.

According to previous studies, there are two possible factors affecting the void-induced swelling. Mansur et al. [35] proposed a key parameter expression affecting the growth of voids, as shown in Eq. (1), which considers the sink strength of defects.

$$dR/dt = \frac{\Omega D_i D_V}{2RK_i^V}\left[\left(1 + \frac{4K_i^V K_0}{D_i D_V S_i S_V}\right)^{1/2} - 1\right](Z_V S_V - Z_i S_i)$$

(1)

where R is the radius of voids, Ω is the atomic volume, and S_i and S_V are sink strengths of interstitials and vacancies. D_i and D_V are the diffusion coefficients of interstitials and vacancies. K_0 and $(Z_V - Z_i)$ are the temperature-independent formation rate of defects and the dislocation bias factor, respectively. K_i^V is the recombination or annihilation rate of point defects. In this case, according to the sign of $(Z_V S_V - Z_i S_i)$ in

Eq. (1), the voids may be growing or shrinking. Furthermore, the greater the sink strength (S_i and S_V) is, the slower the swelling rate is, because point defects are absorbed by the sinks rather than being voids. Interstitial carbon can be considered as absorption sinks for self-interstitials and vacancies. On the one hand, it is because carbon atoms provide the sites where self-interstitials or clusters nucleate as dislocation loops, thereby absorbing lots of self-interstitials. On the other hand, interstitial carbon could combine with vacancies to form C-vacancy complexes and hinder the movement of vacancies. The experimental results and theoretical analysis above indicate that interstitial carbon could increase the sink strength of HEAs; that is, it absorbs self-interstitials atoms and vacancies and promotes their recombination and annihilation. However, a bulk of black dots were observed in TEM images, which are considered as interstitial clusters or small-sized dislocation loops. Therefore, if we consider the influence of interstitial clusters and their mobility on Eq. (1),

then the equation can be transformed into (2) and (3) [36, 37].

$$dS/dt = \left(D_v C_v z_v^v\right) k_v^2 - D_g C_g x_g k_g \pi R_v^2 \rho_v \qquad (2)$$

$$dS/dt = K_0^{\text{eff}} \left[\varepsilon_i^g \left(\frac{Z_v^V k_v^2}{Z_v^V k_v^2 + Z_v^d \rho_d} - \frac{\pi R_V^2 \rho_V}{k_g} \right) \right.$$
$$\left. + (1 - \varepsilon_i^g) P_1 \frac{Z_v^V k_v^2 Z_v^d \rho_d}{\left(Z_i^V k_v^2 + Z_i^d \rho_d \right) \left(Z_v^V k_v^2 + Z_v^d \rho_d \right)} \right]$$
$$(3)$$

where D_g and C_g are the diffusion coefficient and concentration of interstitial clusters. x_g is the size of the cluster. The perturbation of cluster recombination is ignored, and Eq. (2) is expanded to obtain Eq. (3). There are three key parameters in Eq. (3), which are the efficiency of Frenkel pairs K_0^{eff}, the proportion of the 1D migration of interstitial clusters ε_i^g, and the proportion of clusters that migrate in 3D path $(1 - \varepsilon_i^g)$. Considering the same irradiation condition and similar alloy components, the efficiency of defect pairs remains unchanged in our work. Under this premise, the factor affecting swelling rate is the migration (1D or 3D path) of interstitial clusters. In HEAs, most interstitial clusters exhibit 3D migrations, which can also be confirmed in the TEM results in our work. Thus, the value of ε_i^g is negligible. The cluster size observed in TEM decreases with increasing carbon content, indicating that the absorption intensity of voids to point defects ($Z_i^V k_v^2$) is improved. Moreover, no voids were found in all the irradiated samples, which means that the void bias of all the samples can be considered as the same value. Therefore, the value of the last term on the right side of Eq. (3) decreases as the carbon content increases, indicating the decrease in swelling rate. In this way, we explain why the sample swelling rate decreases with the increasing carbon content from a theoretical perspective.

Carbon doping would increase the migration energy of point defects, which is conducive to the nucleation but not to the growth of dislocation loops. Studies have shown that the reduced mobility of dislocation loops would suppress irradiation swelling [38, 39]. Considering the inherent sluggish
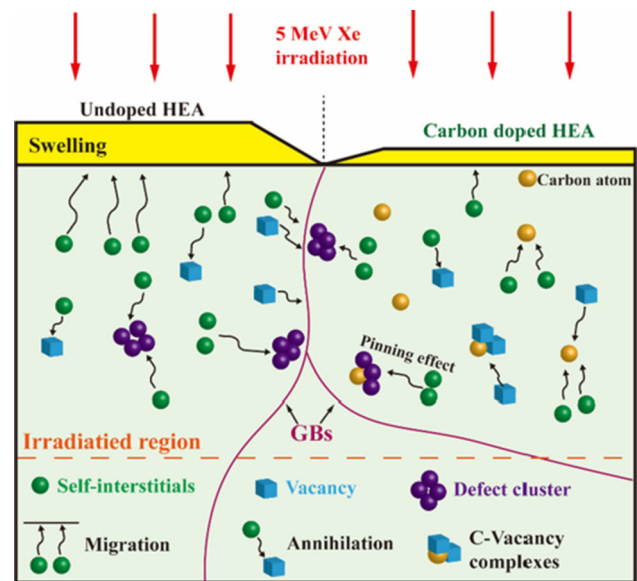

Figure 8 Schematic of the evolution of irradiation-induced defects in HEAs with and without carbon doping. The case of undoped HEA is shown on the left, and the carbon-doped HEAs are on the right. The orange balls on the right represent interstitial carbon atoms.

diffusion effect in HEAs, carbon doping may further aggravate lattice distortion and significantly reduce the migration rate of interstitial atoms. Therefore, a large number of uncaptured interstitial atoms would provide numerous recombination positions for vacancies, promoting the annihilation of interstitial atoms and vacancies. Meanwhile, octahedral interstitial carbon atoms have a pinning effect on irradiation-induced interstitial atom clusters and dislocation loops, which hinders the accumulation and growth of irradiation-induced defects. Furthermore, interstitial carbon atoms could combine with vacancies and form C-vacancy complexes, which would inhibit the evolution of vacancies and hinder the growth of voids even at elevated temperatures. As shown in Fig. 8, it is believed that the recombination of the defects significantly reduces the number of interstitial atoms migrating to the surface, and the pinning effect of interstitial carbon on clusters inhibits the growth of irradiation-induced defects, thereby reducing the swelling of the carbon-doped HEAs irradiated at 500 °C in our work.

Conclusion

In this study, the irradiation-induced defects and swelling in $Fe_{38}Mn_{40}Ni_{11}Al_4Cr_7$ HEAs with different carbon contents were compared at 300 °C and 500 °C with 5 MeV Xe^{23+} ions irradiated to a fluence of 1.4×10^{15} cm^{-2}. TEM and AFM were used to provide essential evidence. On this basis, we revealed the effects of interstitial carbon on the irradiation resistance of HEAs at elevated temperature and discussed the evolution of irradiation-induced defects and swelling of carbon-doped HEAs at different temperatures. This study shows the positive effects of carbon doping on irradiation resistance and provides theoretical and experimental bases for the potential of carbon-doped HEAs as reactor structural materials. The specific research conclusions are as follows:

1. Both in the case of 300 °C and 500 °C irradiation, carbon-doped HEAs exhibited smaller and denser irradiation-induced dislocation loops than the undoped HEAs. This phenomenon may be attributed to the pinning effect of interstitial carbon on dislocation loops, which hinders the accumulation and growth of irradiation defects.

2. In the case of HEAs with the same carbon content, elevated temperature would promote the growth of irradiation-induced dislocation loops, resulting in the larger-sized and lower-density dislocation loops in HEAs irradiated at 500 °C than those under the 300 °C irradiation condition.

3. At a low irradiation temperature (300 °C), the inhibitory effects of interstitial carbon on the dislocation loops are mainly manifested in promoting the recombination of defects and the pinning effect on dislocation loops. However, in the case of 500 °C irradiation, the pinning effect of interstitial carbon is weakened due to the increased mobility of carbon atoms at elevated temperature, resulting in the nearly constant size of dislocation loops with the changing carbon content.

4. Under the 500 °C irradiation condition, swelling was observed on both sides of the grain boundaries in the irradiated samples, while no detectable swelling was found at 300 °C irradiation. The swelling at 500 °C decreased with the increase in carbon content. This is attributed to the reason that interstitial carbon atoms hindered the long-distance migration of self-interstitials, promoted the recombination of Frenkel pairs, and reduced the number of self-interstitials that can move to the surface and cause swelling.

References

[1] Jin K, Lu C, Wang L, Qu J, Weber WJ, Zhang Y, Bei H (2016) Effects of compositional complexity on the ion-irradiation induced swelling and hardening in Ni-containing equiatomic alloys. Scripta Mater 119:65–70

[2] Lin JW, Chen FD, Tang XB, Liu J, Shen SK, Ge GJ (2020) Radiation-induced swelling and hardening of 316L stainless steel fabricated by selected laser melting. Vacuum 174:109183

[3] Holmes JJ, Robbins RE, Brimhall JL, Mastel B (1968) Elevated temperature irradiation hardening in austenitic stainless steel. Acta Mater 16(7):955–967

[4] Was GS, Ashida Y, Andresen PL (2011) Irradiation-assisted stress corrosion cracking. Corros Rev 29:7–49

[5] Tsai MH, Yeh JW (2014) High-entropy alloys: a critical review. Mater Res Lett 2(3):107–123

[6] Zhang WR, Liaw PK, Zhang Y (2018) Science and technology in high-entropy alloys. Sci China Mater 61(1):2–22

[7] Yang L, Ge H, Zhang J, Xiong T, Jin QQ, Zhou Y, Shao XH, Zhang B, Zhu Z, Zheng SJ, Ma XL (2019) High He-ion irradiation resistance of CrMnFeCoNi high-entropy alloy

revealed by comparison study with Ni and 304SS. J Mater Sci Technol 35(3):300–305

[8] Egami T, Guo W, Rack PD, Nagase T (2014) Irradiation Resistance of Multicomponent Alloys. Metall Mater Trans A 45(1):180–183

[9] Yang T, Xia S, Guo W, Hu R, Poplawsky JD, Sha G, Fang Y, Yan Z, Wang C, Li C et al (2018) Effects of temperature on the irradiation responses of Al 0.1 CoCrFeNi high entropy alloy. Scripta Mater 144:31–35

[10] Yang TN, Lu CY, Velisa G, Jin K, Xiu PY, Zhang YW, Bei HB, Wang LM (2019) Influence of irradiation temperature on void swelling in NiCoFeCrMn and NiCoFeCrPd. Scripta Mater 158:57–61

[11] Yang TF, Xia SQ, Liu S, Wang CX, Liu SS, Fang Y, Zhang Y, Xue JM, Yan S, Wang YG (2016) Precipitation behavior of Al$_x$CoCrFeNi high entropy alloys under ion irradiation. Sci Rep 6:32146

[12] Guo Z, Zhang A, Han J, Meng J (2019) Effect of Si additions on microstructure and mechanical properties of refractory NbTaWMo high-entropy alloys. J Mater Sci 54(7):5844–5851. https://doi.org/10.1007/s10853-018-03280-z

[13] Stepanov ND, Shaysultanov DG, Chernichenko RS, Yurchenko NY, Zherebtsov SV, Tikhonovsky MA, Salishchev GA (2017) Effect of thermomechanical processing on microstructure and mechanical properties of the carbon-containing CoCrFeNiMn high entropy alloy. J Alloys Compd 693:394–405

[14] Wang Z, Bei H, Baker I (2018) Microband induced plasticity and the temperature dependence of the mechanical properties of a carbon-doped FeNiMnAlCr high entropy alloy. Mater Charact 139:373–381

[15] Li JB, Gao B, Tang S, Liu B, Liu Y, Wang Y, Wang JW (2018) High temperature deformation behavior of carbon-containing FeCoCrNiMn high entropy alloy. J Alloys Compd 747:571–579

[16] Lu E, Makkonen I, Mizohata K, Li Z, Räisänen J, Tuomisto F (2020) Effect of interstitial carbon on the evolution of early-stage irradiation damage in equi-atomic FeMnNiCoCr high-entropy alloys. J Appl Phys 127:025103

[17] Shen S, Chen F, Tang X, Lin J, Ge G, Liu J (2020) Effects of carbon doping on irradiation resistance of Fe38Mn40-Ni11Al4Cr7 high entropy alloys. J Nucl Mater 540:152380

[18] Lu CY, Niu LL, Chen NJ, Jin K, Yang TN, Xiu PY, Zhang YW, Gao F, Bei HB, Shi S, He MR, Robertson IM, Weber WJ, Wang LM (2016) Enhancing radiation tolerance by controlling defect mobility and migration pathways in multicomponent single-phase alloys. Nat Commun 7:13564

[19] Wolff J, Franz M, Kluin JE, Schmid D (1997) Vacancy formation in nickel and α-nickel-carbon alloy. Acta Mater 45(11):4759–4764

[20] Cermak J, Kral L (2014) Effect of carbon-supersaturation upon the carbon diffusion in 9Cr–1Mo ferrite steel. Mater Lett 116:402–404

[21] Kresse T, Borchers C, Kirchheim R (2013) Vacancy–carbon complexes in bcc iron: correlation between carbon content, vacancy concentration and diffusion coefficient. Scripta Mater 69(9):690–693

[22] Wang Z, Baker I, Cai Z, Chen S, Poplawsky JD, Guo W (2016) The effect of interstitial carbon on the mechanical properties and dislocation substructure evolution in Fe$_{40.4}$Ni$_{11.3}$Mn$_{34.8}$Al$_{7.5}$Cr$_6$ high entropy alloys. Acta Mater 120:228–239

[23] Wang Z, Baker I (2016) Interstitial strengthening of a f.c.c. FeNiMnAlCr high entropy alloy. Mater Lett 180:153–156

[24] Ehrhart P, Averback RS (1989) Diffuse X-ray scattering studies of neutron- and electron-irradiated Ni, Cu and dilute alloys. Philos Mag A 60(3):283–306

[25] Theis U, Wollenberger H (1980) Mobile interstitials produced by neutron irradiation in copper and aluminium. J Nucl Mater 88(1):121–130

[26] Tsai KY, Tsai MH, Yeh JW (2013) Sluggish diffusion in Co–Cr–Fe–Mn–Ni high-entropy alloys. Acta Mater 61(13):4887–4897

[27] Bae DS, Nahm SH, Lee HM, Kinoshita H, Shibayama T, Takahashi H (2004) Effect of electron-beam irradiation temperature on irradiation damage of high Mn–Cr steel. J Nucl Mater 329–333:1038–1042

[28] Zinkle SJ, Maziasz PJ, Stoller RE (1993) Dose dependence of the microstructural evolution in neutron-irradiated austenitic stainless steel. J Nucl Mater 206(2–3):266–286

[29] Terentyev D, Martin-Bragado I (2015) Evolution of dislocation loops in iron under irradiation: the impact of carbon. Scripta Mater 97:5–8

[30] Hepburn DJ, Ferguson D, Gardner S, Ackland GJ (2013) First-principles study of helium, carbon, and nitrogen in austenite, dilute austenitic iron alloys, and nickel. Phys Rev B 88(2):024115

[31] Arakawa K, Hatanaka M, Mori H, Ono K (2004) Effects of chromium on the one-dimensional motion of interstitial-type dislocation loops in iron. J Nucl Mater 329–333:1194–1198

[32] Terasawa M, Mitamura T, Liu L, Tsubakino H, Niibe M (2002) Metal surface swelling by heavy charged particle irradiation. Nucl Instrum Methods B 193:329–335

[33] Little EA, Stow DA (1979) Void-swelling in irons and ferritic steels: II. An experimental survey of materials irradiated in a fast reactor. J Nucl Mater 87(1):25–39

[34] Shimada M, Nakahigashi S, Terasawa M (1975) On the surface denudation of voids induced by 200 keV C+ ion irradiation. Radiat Eff Defects Solids 25(4):283–285

[35] Mansur LK (1994) Theory and experimental background on dimensional changes in irradiated alloys. J Nucl Mater 216:97–123

[36] Singh BN, Golubov SI, Trinkaus H, Serra A, Osetsky YN, Barashev AV (1997) Aspects of microstructure evolution under cascade damage conditions. J Nucl Mater 251:107–122

[37] Golubov SI, Singh BN, Trinkaus H (2000) Defect accumulation in fcc and bcc metals and alloys under cascade damage conditions: Towards a generalisation of the production bias model. J Nucl Mater 276(1):78–89

[38] Terentyev D, Olsson P, Malerba L, Barashev AV (2007) Characterization of dislocation loops and chromium-rich precipitates in ferritic iron-chromium alloys as means of void swelling suppression. J Nucl Mater 362(2):167–173

[39] Garner FA, Toloczko MB, Sencer BH (2000) Comparison of swelling and irradiation creep behavior of fcc-austenitic and bcc-ferritic/martensitic alloys at high neutron exposure. J Nucl Mater 276(1):123–142